

Synthesis and Characterization of Ferric Vanadate Nanorods for Efficient Electrochemical Detection of Ascorbic Acid

Nadia Anwar,^{††} Muhammad Munir Sajid,^{††} Muhammad Aamir Iqbal,^{*} Haifa Zhai, Muqarrab Ahmed, Bushra Anwar, Kareem Morsy, Rey Y. Capangpangan, Arnold C. Alguno, and Jeong Ryeol Choi^{*}



Cite This: *ACS Omega* 2023, 8, 15450–15457

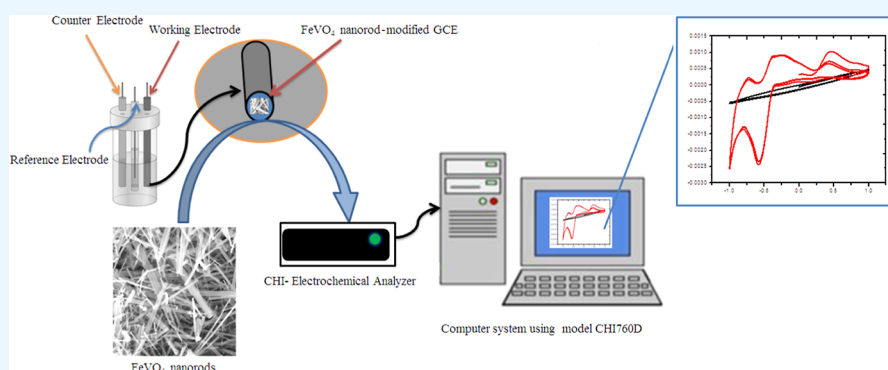


Read Online

ACCESS |

Metrics & More

Article Recommendations



ABSTRACT: This study reports the synthesis of ferric vanadate (FeVO_4) via a facile hydrothermal method, focusing on demonstrating its exceptional electrochemical (EC) properties on detecting low-density ascorbic acid (AA). The phase purity, crystallinity, structure, morphology, and chemical compositional properties were characterized by employing X-ray diffraction, energy-dispersive X-ray spectroscopy, scanning electron microscopy, Raman spectroscopy, and X-ray photoelectron spectroscopy techniques. EC impedance spectroscopy and cyclic voltammetry techniques were also adopted in order to assess the EC response of a FeVO_4 -modified glassy carbon electrode for sensing AA at room temperature. The AA concentration range adopted in this experiment is 0.1–0.3 mM at a working electric potential of -0.13 V. The result showed functional excellence of this material for the EC determination of AA with good stability and reproducibility, promising its potentiality in connection with relevant sensing applications.

1. INTRODUCTION

Nanotechnology is a powerful platform as electro-analytical facilities¹ in high-sensitivity morphological characterization of nanoscale materials.^{2–4} A large number of metal oxides, polymers, carbon materials, and nanomaterial complexes with diverse structures have been adopted in engineering, especially for the purpose of their applications as electrochemical (EC) sensors.^{5–7} Among them, ternary metal vanadate-like orthovanadate (MVO_4) nanomaterials have involved significant consideration owing to their effective chemical and physical properties for various practical uses in the disciplines of EC sensors, solar cells, capacitive deionization, photocatalysis, magnetic devices, and lithium batteries.⁸ So far, EC characteristics of various vanadates, such as BiVO_4 ,⁹ AgVO_4 ,¹⁰ CuVO_4 ,¹¹ EuVO_4 ,¹² NdVO_4 ,¹³ and LaVO_4 ,¹⁴ have been reported in the literature. Using a straightforward sonochemical process, BiVO_4 was produced from metal precursors such as bismuth and vanadium.¹⁵ Lakshmana Naik and Bala Narsaiah reported that $\text{Zn}_2\text{V}_2\text{O}_7$ can be synthesized by employing a hydrothermal method on the graphene oxide

scaffolds.¹⁶ The literature¹⁷ also reports the synthesis of CeVO_4 nanoparticles by using a variety of techniques, such as ultrasonic, hydrothermal, sol–gel, coprecipitation, microwave irradiation, solvothermal, and sonochemical methods. Although the majority of these methods can produce CeVO_4 nanoparticles with precise sizes and shapes, the hydrothermally produced $\text{Co}_3\text{V}_2\text{O}_8$ thin nanoplates were reported to work well as cathode materials for LiBs.¹⁸ As a typical class of metal vanadate, nanostructured FeVO_4 is especially noticeable as an active material in Fenton-like catalysts, electrochromic electrodes, and rechargeable Li-ion batteries.¹⁹ In these reported investigations, the bottom-up, hydrothermal method was

Received: February 3, 2023

Accepted: April 12, 2023

Published: April 21, 2023



employed for preparing nanostructures, mainly due to the advantages of adjustable parameters and low working temperature, admitting inexpensive, linear synthesis, and fine electric attributes with potential for mass production of superior sensors, commonly not achievable through conventional solid-state chemical reactions.^{20,21}

Transition-metal vanadates (MV_xO_y), which are related to V_2O_5 , have recently attracted more attention in a variety of fields due to their layered structure and distinctive physical, chemical, and electrical properties. $FeVO_4$ is a typical N-type semiconductor and a very stable material. It possesses exceptional EC and catalytic properties that make it a good candidate for sensor development. Additionally, iron (Fe) and vanadium (V) have an indirect band gap and a better redox reaction compared to other metal vanadates, making them an excellent choice for a variety of EC applications.²² Using a hydrothermal process, Che et al. produced Pb-doped $FeVO_4$ nanotubes that respond to ethanol at 200 ppm.²³ It has been predicted that the sensing properties of nanosized $FeVO_4$ would be better than those of bulk $FeVO_4$ since the sensitivity of a sensor material greatly depends on surface qualities.²⁴ The utilization of electrode materials for enhanced energy storage applications calls for the usage of layered alkali-containing 3d transition-metal oxides.²⁵

Ascorbic acid (AA) is a water-soluble organic vitamin that is required for catalyzing enzymatic responses and defense mechanisms against various diseases and oxidative stress.^{26,27} It is also essential in human body-metabolic development, including certain hormones, anti-inflammatory steroids, differentiation of cells, collagen synthesis, and amino acid metabolism.^{28,29} Therefore, it is necessary to detect AA under complex conditions, and many techniques have already been reported for the selective and sensitive EC detection of AA. Nevertheless, high-performance novel nanocomposites with ever-demanding sensitivity and application-friendly linear sensing responses have yet to be industrialized.^{30,31}

Our objective in this research is to unveil the sensitivity detection applications of ferric vanadate nanorods synthesized via a facile hydrothermal synthetic technique, which utilizes ammonia metavanadate and ferric nitrate as crude precursors, polyvinylpyrrolidone (PVP) as a surface-active agent, and NaOH to adjust pH values. Ferric vanadate has been adopted to modify the glassy carbon electrode (GCE) in order to improve its EC response against AA. We will show that it works with a low detection limit across a wide linear range for AA determination, proving that it is a potential candidate for application in biosensing and some other sensors.

2. EXPERIMENTAL ILLUSTRATION

2.1. Materials and Methods. All the reagents utilized in this study were of analytical grade, obtained from Sigma-Aldrich and Merck distributors, and were not further purified before use. The schematic step-by-step mechanism for the synthesis of $FeVO_4$ nanorods by employing a hydrothermal mechanism is depicted in Figure 1. For the preparation of $FeVO_4$ nanorods, a stoichiometric quantity of 7.096 g of high-purity iron(III) nitrate [$Fe(NO_3)_3 \cdot 9H_2O$, 98% Sigma-Aldrich], 2.052 g of ammonium metavanadate (NH_4VO_3 , 99.95% PubChem), NaOH (0.702 g, 99.99% PubChem), and 0.400 g of PVP [$(C_6H_9NO)_n$, 97% Sigma-Aldrich] were liquified in double-distilled water. Under magnetic stirring, liquified aqueous iron(III) nitrate [$Fe(NO_3)_3 \cdot 9H_2O$] was added to 10 mL of Triton X-100 in 100 mL of distilled water. Then,

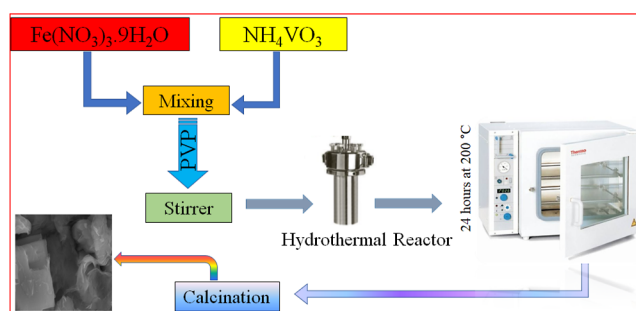


Figure 1. Schematic illustration for the preparation of $FeVO_4$ nanorods.

NH_4VO_3 was imparted, whereas the pH of the solution was accustomed to 8 by consuming NaOH solution. The above solution was stirred for another half hour before being kept at 200 °C in the furnace for 24 h. To remove impurities, the resulting products were washed numerous times with distilled water as well as ethanol before being dried at 80 °C for 6 h. Finally, the materials were calcined for 3 h at 600 °C to get the final samples for further characterization.³² In this study, $FeVO_4$ nanorods were used as a modified GCE working electrode for electrode adjustment. First, $FeVO_4$ (0.5 mg) was dispersed in 1 mL of distilled water, and then 10 μ L of nanomaterial was placed on the GC electrodes and dehydrated in an oven at 80 °C for 2 min. After that, 2–3 μ L of 5% Nafion was drop-cast onto the electrodes and dried out. The appropriate concentrations were obtained through appropriate dilutions of the associated stock solutions, and each sensor-reading solution was made from distilled water. The $FeVO_4$ -modified glassy electrode was applied as the working electrode, a carbon glassy rod as the counter electrode, and a saturated calomel electrode (SCE) as the reference electrode. The GCE was initially carefully washed with a substantial amount of DI water/ethanol to eliminate impurities from the electrode surface, and then the electrode was dried in a typical environment. A GCE was drop-cast with an optimal amount of $FeVO_4$ suspension and let to dry in a hot air oven at 50 °C. The altered electrode was subsequently used for EC impedance spectroscopy (EIS) and cyclic voltammetry (CV) analysis.

2.2. Characterization of $FeVO_4$ Nanorods. The crystal structure, as well as phase purity of prepared nanorods, was evaluated using the X-ray diffraction (XRD) method by employing the Rigaku 2500 X-ray diffractometer with Cu $K\alpha$ radiation ($\lambda = 0.15406$ nm) in the angle range of $20^\circ < 2\theta < 60^\circ$. The morphological analysis of particles was done by scanning electron microscopy (SEM, JSM-6460, Japan) functioning at a working voltage of 20 kV, while energy-dispersive X-ray (EDX) spectroscopy was employed to examine the elemental compositional analysis of the nanorods. Raman analysis was carried out by using the excitation source of a 532 nm laser at room temperature and a Lab-RAM, HR Evolution (HORIBA Scientific).

2.3. Sensor Measurements. The EC evaluation of the synthesized material was carried out via the use of the CHI-760D EC working station. The working electrode in this experiment was the $FeVO_4$ nanorod-modified GCE, wherein a platinum plate was employed as the counter electrode and an SCE at a potential of -0.13 V as the reference electrode. The material was also analyzed using EIS with a 10 mV amplitude at frequencies between 0.1 and 4000 Hz. We also obtained a

CV spectrum for a 0.1 M mixed solution of Li_2SO_4 and AA at various concentrations with a voltage value between -1.0 and $+1.0$ V at a potential scan rate of 50 mV s^{-1} . Li_2SO_4 reduced the corrosion of current collectors, wherein electrolytes play an important role in the EC reactions of AA, as do the AA concentration and the scan rate. In a sensor, an electrolyte acts as a chemical medium for ion change, and an ideal electrolyte should generally exhibit extremely specific qualities in a number of its functionalities that are essential for the sensor, such as thermal stability, nontoxicity, environmental adaptability, adequate ionic conductivity, and EC stability.³³ These measurements were all made in a temperature-neutral environment.

3. RESULTS AND DISCUSSION

3.1. Morphological Analysis. The field-emission SEM (FESEM) pictures of FeVO_4 nanorods fabricated by a facile hydrothermal method at different magnifications are depicted in Figure 2, where adopted magnification is $1 \mu\text{m}$ for Figure 2a

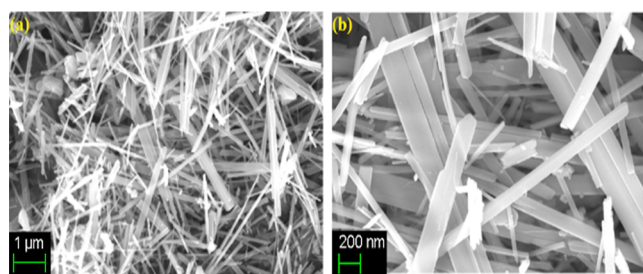


Figure 2. SEM images of hydrothermally prepared FeVO_4 nanorods prepared at 180°C at different magnifications: (a) $1 \mu\text{m}$ and (b) 200 nm .

and 200 nm for Figure 2b. The FESEM images of the samples clearly show the formation the nanorods. The low dimensionality of the surface structures of these rods makes them ideal for containing a huge number of active sites with the purpose of inducing a strong catalytic activity. The range of average diameter calculated from these micrographs is around $\sim 30\text{--}60 \text{ nm}$. These nanorods will definitely improve the activity as there is a higher surface area necessary for reactions associated with a rapid oxidation and reduction response.

3.2. Compositional Analysis. For the compositional characterization of the as-prepared FeVO_4 nanorods, their chemical elements were analyzed using the EDX results, which are shown in Figure 3. They indicate that the byproduct comprises only Fe (12.63%), V (38.80%), O (26.43%), C (12.93%), and Pt (9.20%), which is because of the carbon tape and Pt coating. As far as the detection limit is concerned, there were no additional impurities found.

3.3. XRD Analysis. The XRD pattern for FeVO_4 nanorods can be seen in Figure 4. The cell's measured lattice parameters

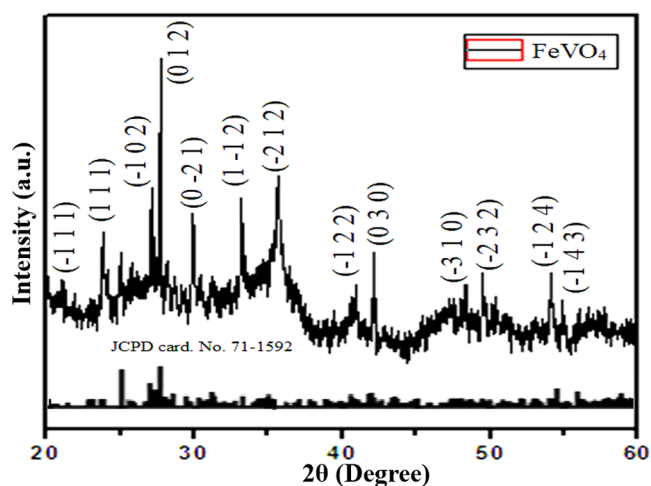


Figure 4. XRD patterns of as-synthesized FeVO_4 nanorods.

are $a = 6.72 \text{ \AA}$, $b = 8.07 \text{ \AA}$, and $c = 9.26 \text{ \AA}$, indicating that the samples exhibit a triclinic crystal structure. They correspond to the case of all pure FeVO_4 diffraction peaks in the anorthic phase, which are nicely matched to the cited JCPD card with no. 71-1592: this number is equivalent to (-111) , (-102) , (012) , $(0-21)$, $(1-12)$, (-212) , (-122) , (030) , $(2-21)$, (-213) , (-310) , (-232) , $(-1-24)$, $(-1-43)$, and (-412) reflections. In an anorthic system, neither sides nor angles are observed to be equivalent to one another, namely, $a \neq b \neq c$ and $\alpha \neq \beta \neq \gamma$. The XRD pattern shows the development of various diffraction peaks related to the FeVO_4 compound, manifesting the synthesis of FeVO_4 nanostructures having rod shapes. The strong peak is observed at $2\theta = 27.7055^\circ$, which is

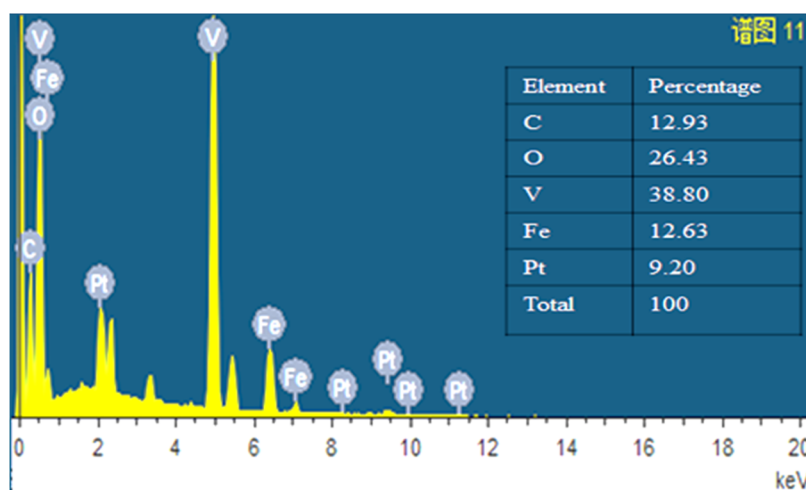


Figure 3. EDX image of FeVO_4 confirming the elemental composition in the sample.

associated with the (1–12) plane. Within the detection limit, no impurity phase has been seen in the XRD patterns, and these XRD peak patterns match well with the existing literature.³² The higher peaks of intensity reveal the high crystallinity of the catalyst, which is favorable from the view of the sensing capacity tied to the resulting improvement of the response.

3.4. Raman Spectroscopy Analysis. Raman spectroscopy is a useful tool for elemental analysis of molecules' vibrational modes. The Raman spectra shown in Figure 5 for FeVO₄

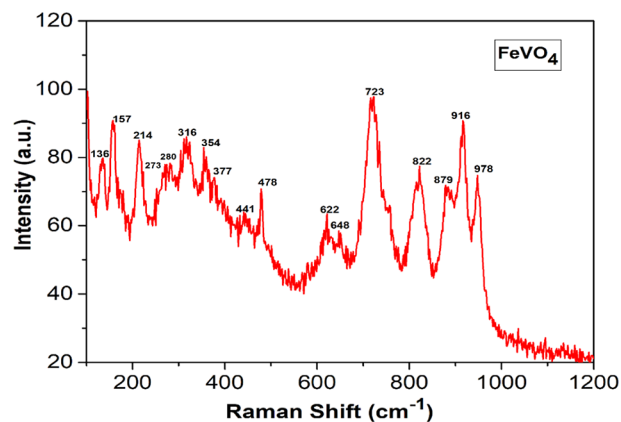


Figure 5. Raman spectra of the prepared FeVO₄ nanorods.

nanorods can be classified into four main groups based on the Raman peak size, in which 970–895 cm⁻¹ relates to V–O stretching at the terminal, 890–736 cm⁻¹ for bridging over V–O–Fe stretching, 730–632 cm⁻¹ relates to mixed bridging between V–O–Fe and V–O–Fe stretching, and 502–317 cm⁻¹ relates to related V–O–V deformations and Fe–O stretching. By comparing them with the values that appear in the literature, every band belongs to one of these specific groups.³⁴

3.5. XPS Analysis. The surface chemical environment and valence state of FeVO₄ for different elements present were evaluated by X-ray photoelectron spectrometry (XPS). Figure 6a demonstrates that the main elements composing the samples are iron (Fe), vanadium (V), and oxygen (O) as expected. Fe ions in Fe²⁺ forms are confirmed by the Fe 2p (see Figure 6b) spectra's two conspicuous peaks at 711.27 and 723.34 eV, which match two bands for Fe 2p_{3/2} and Fe 2p_{1/2}, respectively. The V⁵⁺ oxidation states are shown in Figure 6c: peaks at 516.68 eV are consistent with V 2p_{3/2} and a peak at 523.49 eV is consistent with V 2p_{1/2}. The XPS spectrum of O 1s is displayed in Figure 6d, where the corresponding peak at 530.41 eV is ascribed to metal oxide groups. This analysis provides even more support for the discrimination of the FeVO₄ composite and edges out our previous XRD, EDX, and Raman results.

3.6. BET Measurements. The Brunauer–Emmett–Teller (BET) measurement was executed in order to estimate the surface area of the FeVO₄ nanorods. The nitrogen adsorption–

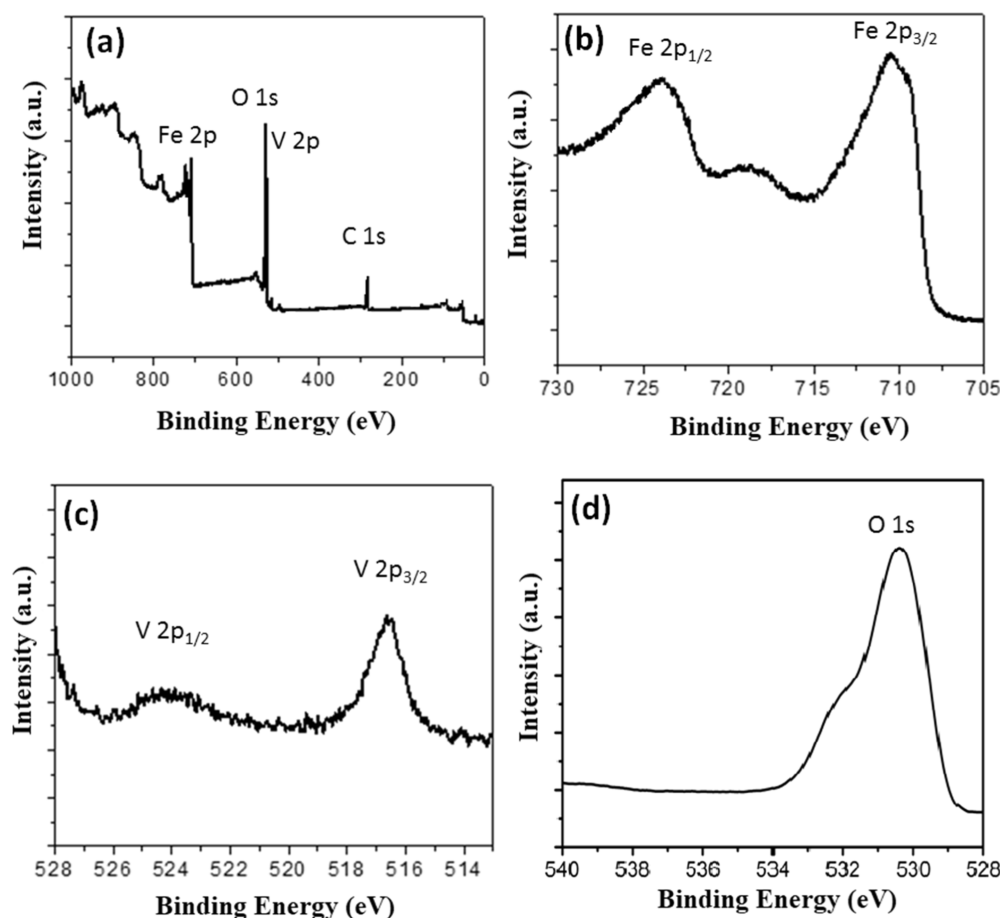


Figure 6. XPS spectra of FeVO₄: (a) outline of the overall main peaks, (b) Fe 2p, (c) V 2p, and (d) O 1s.

desorption patterns for surface area measurements are presented in Figure 7. The surface area measured by the BET technique is about $32.2 \text{ m}^2 \text{ g}^{-1}$, whereas higher values can further enhance electron-transfer kinetics as per the relevant literature.³⁵

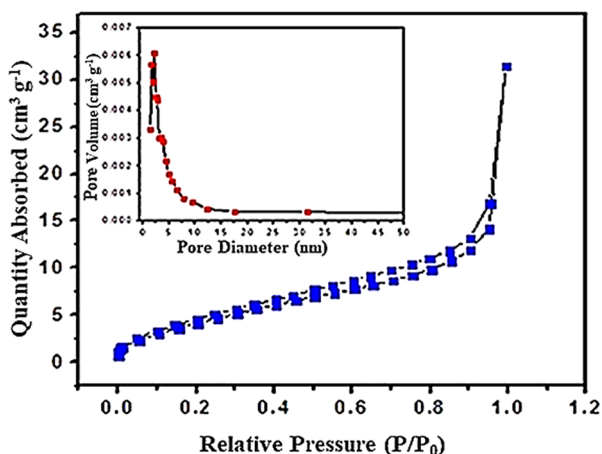


Figure 7. The main graphics (the inset) is the variation of the surface area depending on the relative pressure (the pore diameter) for the FeVO₄ nanorods, where the data are measured with the BET technique.

The pore size was calculated using the Barret–Joyner–Halender method and the desorption isotherms.³⁵ Additionally, the average pore diameter was measured as 2.183 nm and the pore volume was calculated as $0.0061 \text{ cm}^3 \text{ g}^{-1}$. There is a type-III curve observed for adsorption with an H₃-type hysteresis, which is associated with wedged-shaped pores. The lamellar pore wedge shape of the pores indicates the occurrence of mesopores within the structure. As a result, we conclude that FeVO₄ is a highly crystalline mesoporous material. The mesoporous structures provide more sites for the reaction and can capture more electrons, resulting in highly oxidized states. Because of this, a higher specific area and mesoporous structures are in favor for the functionality of EC sensors.

3.7. EIS Analysis. The technique of EIS is useful for analyzing conduction mechanisms, electron transport, and surface properties of modified GCEs.³⁶ Figure 8 shows the

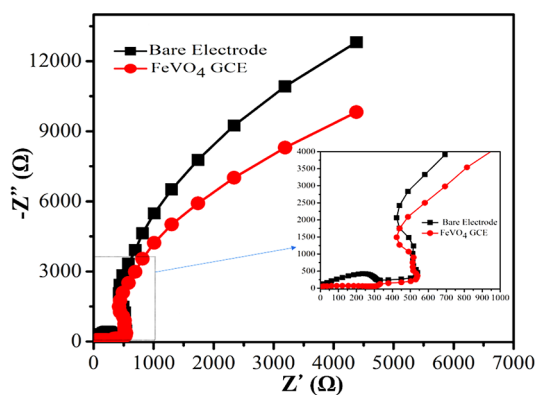


Figure 8. EIS spectra of bare GCE and GCE-modified FeVO₄ nanorods. The inset image clarifies the portion of the semicircle and straight line explained in the text.

differences in EIS spectra between the bare GCE and FeVO₄ nanorod-modified GCE, wherein the spectra of the FeVO₄ nanorod-modified GCE are made up of a curve (or semicircle, if extended) corresponding to a higher value of Z' and a straight line can be seen at a lower value of Z' , as depicted in the inset, wherein Z' and Z'' are the real and imaginary parts of the impedance, respectively. These findings demonstrate that electron-transfer channels at a higher frequency and diffusion at a lower frequency can be used to control the characteristics of the FeVO₄ nanorod-modified GCE. The Nyquist circle diameter of a bare GCE is substantially greater than that of a FeVO₄ nanorod-modified GCE, indicating that the FeVO₄ nanorod-modified GCE has stronger EC activity and better electron transport to the surface than the bare GCE. The FeVO₄ nanorod-modified GCE decreases electron-transfer resistance and provides a good turn in the electron-transfer mechanism.

Figure 9a shows the CV of AA in an assorted solution of 0.1 M Li₂SO₄ and 0.2 mM AA at varying scan rates. It is detected that the intensity of CV peaks (cvp) grows with increasing scan rate from 25 to 200 mV s^{-1} , indicating a linear dependence between scan rate and the current. The correlation coefficient (R) is found to be 0.998 for cvp1 and 0.997 for cvp2, which indicates that the kinetics of the whole action is adsorption process-controlled. This demonstrates that the FeVO₄ nanorod structure is very favorable for anchoring bioactive particles and provides a path for rapid mass transportation.

The detection limit and linear range of AA with the FeVO₄ nanorod-modified GCE were examined by inspecting the CV spectrum of AA in the 0.1–0.3 mM range of concentration within the potential of -1 to $+1$ V. It is noticeable that there is an upsurge in the current intensity in proportion to the increase in the concentration of AA, as seen in Figure 9b. Thus, the intensity of the CV spectrum step ups evidently on raising the quantity of AA. When the dose of AA was varied in the linear range of 0.1–0.3 mM, the coefficient of correlation (R) was observed to be 0.998 and 0.997, and the detection limit was observed as 2.37 and 0.38 μM for cvp1 to cvp2, respectively, at a signal to noise ratio of 3.0, which might be a considerably lower limit of detection. This shows the comparability of analytical efficiency for the detection of AA and a related linear range, so FeVO₄ nanorods provide a platform as a biosensor for the EC detection of AA. Table 1 summarizes a comparison of analytical parameters that are used for the determination of AA using different electrodes involved in these determinations along with the available literature.

The possible detection mechanism for AA can be seen in Figure 10, wherein the reduction reaction occurs at AA and an oxidation reaction occurs at the surface of the FeVO₄ nanorod-modified GCE.



The FeVO₄ nanorod-modified GCE has a large linear range as well as a low detection limit and is an interesting material for EC detection of AA due to its excellent analytical performance. Ferric vanadate nanorods on the surface of the GCE can mediate the heterogeneous chemical oxidation/reduction of the target materials, and the transformed ferric ions can be continually recovered by the EC oxidation/reduction process. Therefore, FeVO₄ nanorods are explored to be employed as

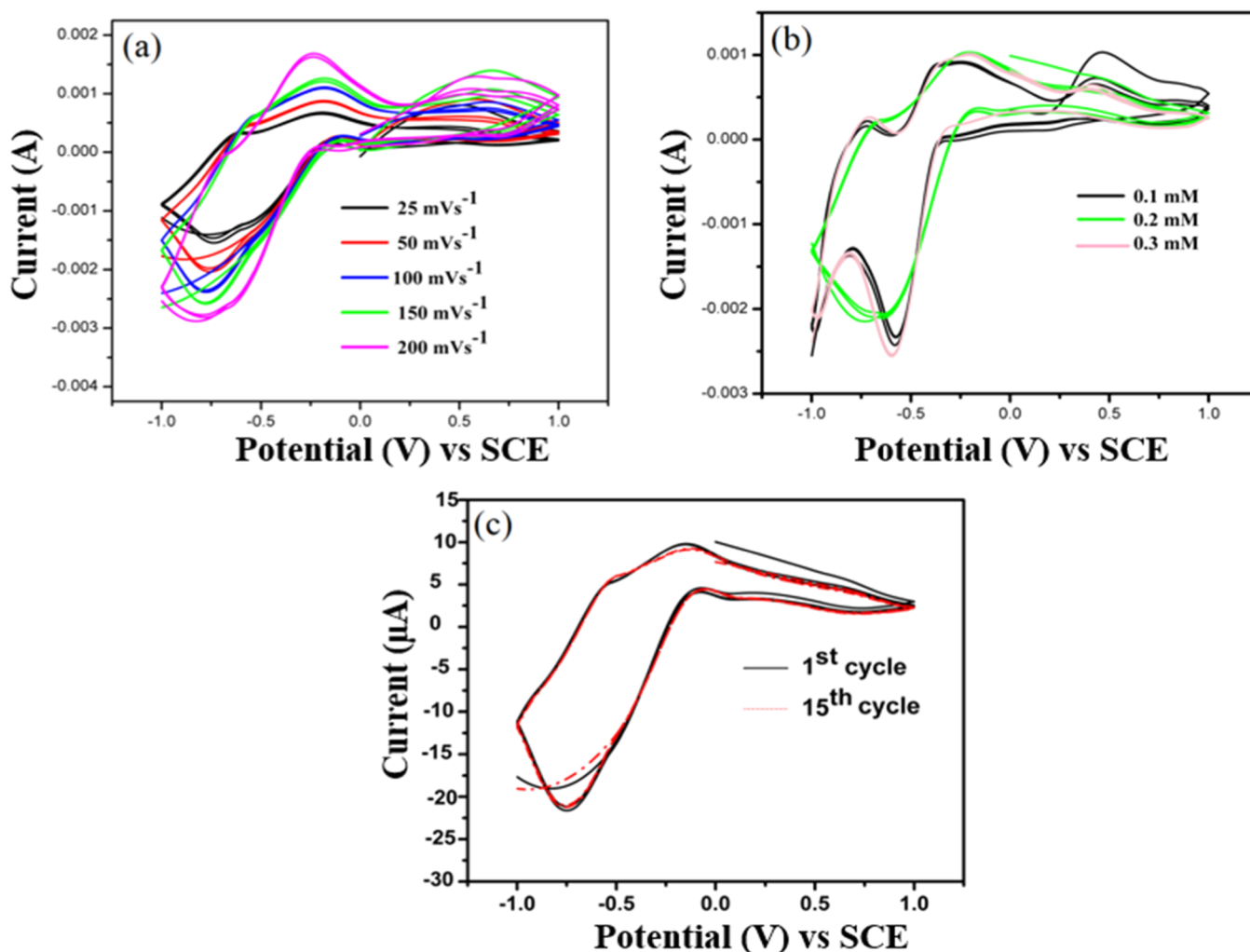


Figure 9. (a) CV peaks of AA at various scan rates, (b) CV peaks of AA at different concentrations, and (c) recycling for 1st and 15th cycle in Li_2SO_4 and AA (0.1 mM) solution at a scan rate of 50 mV s^{-1} .

Table 1. Analysis of the Analytical Parameters for the Determination of AA Using Multiple Electrodes

electrode	linear range (μM)	detection limit (μM)	references
$\text{SnO}_2/\text{graphene}/\text{GCE}$	0.5–200	0.017	37
$\text{GCE}/\text{CNO}-\text{NiMoO}_4-\text{MnWO}_4$	1–100	0.33	38
alginate-/CuO-modified electrode	10–150	1.97	39
MIPs/MXene/GCE	0.5–10	0.27	40
$\text{MoS}_2-\text{RGO}/\text{GCE}$		$\sim 0.43-0.16$	41
FeVO_4/GCE	100–300	0.38	this Work

the GCE-modified materials for the EC detection of AA. The Nyquist circle diameter of a bare GCE is substantially greater than that of a FeVO_4 nanorod-modified GCE, suggesting a high electron transfer on the surface and a decrease in resistance. Overall, adopting a modified GCE improves the electron transport process.

The EC behavior of AA at the FeVO_4 nanorod-modified GCE was studied by using an electrolyte such as LiSO_4 and showed strong oxidation and reduction peaks. For long-term stability and durability, the FeVO_4 nanorod-modified GCE was kept at room temperature for 20 days.⁴² Even so, it was compromised for the detection of AA with no reduction in the

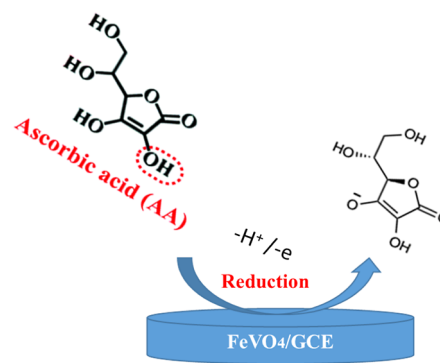


Figure 10. Schematic illustration for the detection of AA using the FeVO_4 nanorod-modified GCE.

current value. It was detected during the experiments that there was no major deviation or change in the morphology of FeVO_4 nanorods with long-term sensing. For reproducibility, AA at 0.1 mM was used for 15 measurements, and the deviation is shown in Figure 9c. Thus, the FeVO_4 nanorod-modified GCE exhibits good stability as well as reproducibility for EC determination of AA.

4. CONCLUSIONS

This study explores the potential of facile autoclave hydrothermally prepared FeVO₄ nanorods for EC detection of AA in the 0.1–0.3 mM range of concentration within the potential range of –1 to +1 V. The fabricated nanorods were elaborately characterized physically and chemically by using advanced analytical techniques such as SEM, EDX, XRD, Raman, BET, and XPS with a reported diameter of nanorods in the range of 30–60 nm. The exquisite size and anorthic phase triclinic crystal morphology of the FeVO₄ nanorod-modified GCE allow detection of low-density AA, and these nanorods could be used as sensitivity detection sensors.

■ ASSOCIATED CONTENT

Data Availability Statement

All data generated or analyzed during this study are included in this article.

■ AUTHOR INFORMATION

Corresponding Authors

Muhammad Aamir Iqbal – School of Materials Science and Engineering, Zhejiang University, Hangzhou 310027, China; orcid.org/0000-0002-5031-5305; Email: maiqbal.research@gmail.com

Jeong Ryeol Choi – School of Electronic Engineering, Kyonggi University, Suwon 16227 Gyeonggi-do, Republic of Korea; Email: choiardor@hanmail.net

Authors

Nadia Anwar – School of Materials Science and Engineering, Tsinghua University, Beijing 100084, China

Muhammad Munir Sajid – Henan Key Laboratory of Photovoltaic Materials, School of Physics, Henan Normal University, Xinxiang 453007, China

Haifa Zhai – Henan Key Laboratory of Photovoltaic Materials, School of Physics, Henan Normal University, Xinxiang 453007, China; School of Materials Science and Engineering, Henan Normal University, Henan 453007, China; orcid.org/0000-0003-2277-1212

Muqarrab Ahmed – State Key Laboratory of Chemical Engineering, Department of Chemical Engineering, Tsinghua University, Beijing 100084, China

Bushra Anwar – Institute of Entomology, Northwest A&F University, Xianyang 712100 Shaanxi, China

Kareem Morsy – Biology Department, College of Science, King Khalid University, Abha 61421, Saudi Arabia

Rey Y. Capangpangan – Department of Physical Sciences and Mathematics, College of Marine and Allied Sciences Mindanao State University at Naawan, Naawan 9023 Misamis Oriental, Philippines

Arnold C. Alguno – Department of Physics, Premier Research Institute of Science and Mathematics (PRISM) Mindanao State University—Iligan Institute of Technology, Iligan City 9200, Philippines

Complete contact information is available at:

<https://pubs.acs.org/10.1021/acsomega.3c00715>

Author Contributions

^{††}N.A. and M.M.S. contributed equally and share the first authorship. N.A.: conceptualization, resources, methodology, writing—original draft preparation, writing—review and editing, and validation. M.M.S.: conceptualization, resources,

methodology, writing—original draft preparation, writing—review and editing, and validation. M.A.L.: conceptualization, resources, methodology, writing—review and editing, and funding acquisition. H.Z.: reviewing, proofreading, validation, and writing—review and editing. M.A.: writing—review and editing and validation. B.A.: writing—review and editing and proofreading. K.M.: reviewing, validation, and funding. R.Y.C.: reviewing, proofreading, and validation. A.C.A.: reviewing, proofreading, and validation. J.R.C.: writing—review and editing, proofreading, validation, and funding acquisition. All authors have read and agreed to the published version of the manuscript.

Notes

The authors declare no competing financial interest.

■ ACKNOWLEDGMENTS

The authors are grateful for the financial support from the Tsinghua University Initiative Scientific Research Program and the Ministry of Science and Technology (MoST). The authors also acknowledge the support provided by Zhejiang University, China, along with the National Research Foundation of Korea (NRF) grant funded by the Korean government (MSIT) (no.: NRF-2021R1F1A1062849), while extending their appreciation to the Deanship of Scientific Research at King Khalid University for supporting this work through large groups (project under grant number R.G.P.2/1/44). Dr. Muhammad Munir Sajid wishes to specially acknowledge Henan Normal University, China, for its financial support.

■ REFERENCES

- (1) Fan, Z.; Jiang, C.; Wang, Y.; Wang, K.; Marsh, J.; Zhang, D.; Chen, X.; Nie, L. Engineered extracellular vesicles as intelligent nanosystem for next-generation of nanomedicine. *Nanoscale Horiz.* **2022**, *7*, 682–714.
- (2) Ramachandran, R. Recent progress and perspective design of various electrode catalysts for the simultaneous determinations of dopamine in the presence of ascorbic acid and uric acid: A review. *Int. J. Electrochem. Sci.* **2017**, *12*, 1572–1588.
- (3) Sharma, N.; Pap, Z.; Garg, S.; Hernadi, K. Photocatalyst composites from Bi-based and carbon materials for visible light photodegradation. *Green Photocatalytic Semiconductors: Recent Advances and Applications*; Springer Nature, 2022; pp 145–178.
- (4) Svehlova, K.; Lukšan, O.; Jakubec, M.; Curtis, E. A. Supernova: a deoxyribozyme that catalyzes a chemiluminescent reaction. *Angew. Chem.* **2022**, *134*, No. e202109347.
- (5) Srivastava, M.; Srivastava, N.; Mishra, P.; Malhotra, B. D. Prospects of nanomaterials-enabled biosensors for COVID-19 detection. *Sci. Total Environ.* **2021**, *754*, 142363.
- (6) Valentini, F.; Ciambella, E.; Boaretto, A.; Rizzitelli, G.; Carbone, M.; Conte, V.; Cataldo, F.; Russo, V.; Casari, C. S.; Chillura-Martino, D. F.; et al. Sensor properties of pristine and functionalized carbon nanohorns. *Electroanalysis* **2016**, *28*, 2489–2499.
- (7) Anakok, D. A.; Cete, S. A New Surface Based on Graphene Modified with Nanoparticles and Nafion for the Detection of Glucose. *Russ. J. Electrochem.* **2021**, *57*, 1186–1195.
- (8) Pei, L.; Wang, S.; Liu, H.; Pei, Y. A review on ternary vanadate one-dimensional nanomaterials. *Recent Pat. Nanotechnol.* **2014**, *8*, 142–155.
- (9) Yu, J.; Kudo, A. Hydrothermal synthesis of nanofibrous bismuth vanadate. *Chem. Lett.* **2005**, *34*, 850–851.
- (10) Holtz, R.; Souza Filho, A.; Brocchi, M.; Martins, D.; Durán, N.; Alves, O. Development of nanostructured silver vanadates decorated with silver nanoparticles as a novel antibacterial agent. *Nanotechnology* **2010**, *21*, 185102.
- (11) Pei, L.; Lin, N.; Wei, T.; Liu, H.; Yu, H. Formation of copper vanadate nanobelts and their electrochemical behaviors for the

- determination of ascorbic acid. *J. Mater. Chem. A* **2015**, *3*, 2690–2700.
- (12) Shandilya, P.; Mittal, D.; Soni, M.; Raizada, P.; Lim, J.-H.; Jeong, D. Y.; Dewedi, R. P.; Saini, A. K.; Singh, P. Islanding of EuVO_4 on high-dispersed fluorine doped few layered graphene sheets for efficient photocatalytic mineralization of phenolic compounds and bacterial disinfection. *J. Taiwan Inst. Chem. Eng.* **2018**, *93*, 528–542.
- (13) Wu, X.; Tao, Y.; Dong, L.; Zhu, J.; Hu, Z. Preparation of single-crystalline NdVO_4 nanorods, and their emissions in the ultraviolet and blue under ultraviolet excitation. *J. Phys. Chem. B* **2005**, *36*, 11544–11547.
- (14) Sun, Y.; Li, C.; Zheng, W. design. Ionic liquid-assisted hydrothermal synthesis of monoclinic structured LaVO_4 nanowires through topotactic transformation from hexagonal $\text{La}(\text{OH})_3$ nanowires. *Cryst. Growth Des.* **2010**, *10*, 262–267.
- (15) Kovenchan, C.; Pandiyarajan, S.; Chen, S. M. Simple sonochemical synthesis of flake-ball shaped bismuth vanadate for voltammetric detection of furazolidone. *J. Alloys Compd.* **2022**, *895*, 162315.
- (16) Lakshmana Naik, R.; Bala Narsaiah, T. Hydrothermal synthesis and characterization of nanocrystalline zinc vanadate ($\text{Zn}_2\text{V}_2\text{O}_7$) on graphene oxide scaffolds. *Mater. Today: Proc.* **2023**, *72*, 268–273.
- (17) Ghotekar, S.; Pansambal, S.; Lin, K.-Y. A.; Pore, D.; Oza, R. Recent advances in synthesis of CeVO_4 nanoparticles and their potential scaffold for photocatalytic applications. *Top. Catal.* **2023**, *66*, 89–103.
- (18) Banerjee, J.; Dutta, K. An overview on the use of metal vanadium oxides and vanadates in supercapacitors and rechargeable batteries. *Int. J. Energy Res.* **2022**, *46*, 3983–4000.
- (19) Lehnen, T.; Valldor, M.; Nižňanský, D.; Mathur, S. Hydrothermally grown porous FeVO_4 nanorods and their integration as active material in gas-sensing devices. *J. Mater. Chem. A* **2014**, *2*, 1862–1868.
- (20) Rasappa, S.; Ghoshal, T.; Borah, D.; Senthamaraiannan, R.; Holmes, J. D.; Morris, M. A. A highly efficient sensor platform using simply manufactured nanodot patterned substrates. *Sci. Rep.* **2015**, *5*, 13270–13311.
- (21) Rasappa, S.; Borah, D.; Faulkner, C. C.; Lutz, T.; Shaw, M. T.; Holmes, J. D.; Morris, M. A. Fabrication of a sub-10 nm silicon nanowire based ethanol sensor using block copolymer lithography. *Nanotechnology* **2013**, *24*, 065503.
- (22) Sun, H.; Li, Y.; Chai, H.; Cao, Y.; Zhou, W. Facile synthesis of cobalt doped nickel vanadate microspheres as battery-type electrode material for hybrid supercapacitor. *J. Alloys Compd.* **2019**, *805*, 388–395.
- (23) Che, Y.; Feng, G.; Guo, W.; Xiao, J.; Song, C. T. Synthesis of FeVO_4 nanoparticles and sensing performance for ethanol gas under different solution pH. *Cryst. Res. Technol.* **2021**, *56*, 2100110.
- (24) Abualdam, S. A. A. *Synthesis and characterization of novel bioplastics by advanced manufacturing techniques*; The University of North Dakota, 2019.
- (25) Hua, W.; Yang, X.; Casati, N. P.; Liu, L.; Wang, S.; Baran, V.; Knapp, M.; Ehrenberg, H.; Indris, S. Probing thermally-induced structural evolution during the synthesis of layered Li-Na-or K-containing 3d transition-metal oxides. *eScience* **2022**, *2*, 183–191.
- (26) Pei, L.; Qiu, F.; Ma, Y.; Lin, F.; Fan, C.; Ling, X.; Zhu, S. Graphene/zinc bismuthate nanorods composites and their electrochemical sensing performance for ascorbic acid. *Fullerenes, Nanotubes, Carbon Nanostruct.* **2019**, *27*, 58–64.
- (27) Ma, Y.; Zhao, M.; Cai, B.; Wang, W.; Ye, Z.; Huang, J. 3D graphene foams decorated by CuO nanoflowers for ultrasensitive ascorbic acid detection. *Biosens. Bioelectron.* **2014**, *59*, 384–388.
- (28) Hameed, S.; Munawar, A.; Khan, W. S.; Mujahid, A.; Ihsan, A.; Rehman, A.; Ahmed, I.; Bajwa, S. Z. Assessing manganese nanostructures based carbon nanotubes composite for the highly sensitive determination of vitamin C in pharmaceutical formulation. *Biosens. Bioelectron.* **2017**, *89*, 822–828.
- (29) Gebretsadik, G.; Seifu, D.; Yimer, G.; Menon, M. K. C. The non-enzymatic antioxidant and level of oxidative stress of tuberculosis patients in selected treatment center in Addis Ababa Ethiopia. *J. Tuberc. Res.* **2015**, *03*, 63–71.
- (30) Castro, R.; Azeredo, L.; Azeredo, M.; De Sampaio, C. S. T. HPLC assay for the determination of ascorbic acid in honey samples. *J. Liq. Chromatogr. Relat. Technol.* **2001**, *24*, 1015–1020.
- (31) Rageh, H.; Abou-Krishna, M.; Abo-Bakr, A.; Abd-Elasabour, M. Electrochemical behavior and the detection limit of ascorbic acid on a Pt modified electrode. *Int. J. Electrochem. Sci.* **2015**, *10*, 4105–4115.
- (32) Sajid, M. M.; Zhai, H.; Shad, N. A.; Shafique, M.; Afzal, A. M.; Javed, Y.; Khan, S. B.; Ikram, M.; Amin, N.; Zhang, Z. Photocatalytic performance of ferric vanadate (FeVO_4) nanoparticles synthesized by hydrothermal method. *Mater. Sci. Semicond. Process.* **2021**, *129*, 105785.
- (33) Zhang, Y.; Pei, L.; Wei, T.; Lin, N. Electrochemical detection of ascorbic acid with aluminium bismuthate nanorods modified electrode. *J. Bionanosci.* **2016**, *10*, 134–139.
- (34) He, X.; Zhang, C.; Tian, D. The structure, vibrational spectra, and thermal expansion study of AVO_4 (A = Bi, Fe, Cr) and $\text{Co}_2\text{V}_2\text{O}_7$. *Materials* **2020**, *13*, 1628.
- (35) Chung, D. Y.; Jun, S. W.; Yoon, G.; Kim, H.; Yoo, J. M.; Lee, K.-S.; Kim, T.; Shin, H.; Sinha, A. K.; Kwon, S. G.; et al. Large-scale synthesis of carbon-shell-coated FeP nanoparticles for robust hydrogen evolution reaction electrocatalyst. *J. Am. Chem. Soc.* **2017**, *139*, 6669–6674.
- (36) Imam, S. S.; Zango, Z. U.; Abdullahis, H. Room temperature synthesis of bismuth oxyiodide with different morphologies for the photocatalytic degradation of norfloxacin. *Am. Sci. Res. J. Eng. Technol. Sci.* **2018**, *41*, 26–39.
- (37) Lavanya, N.; Fazio, E.; Neri, F.; Bonavita, A.; Leonardi, S.; Neri, G.; Sekar, C. Simultaneous electrochemical determination of epinephrine and uric acid in the presence of ascorbic acid using SnO_2 /graphene nanocomposite modified glassy carbon electrode. *Sens. Actuators, B* **2015**, *221*, 1412–1422.
- (38) Saleh Mohammadnia, M.; Marzi Khosrowshahi, E.; Naghian, E.; Homayoun Keihan, A.; Sohoul, E.; Plonska-Brzezinska, M. E.; Rahimi-Nasrabadi, M.; Rahimi-Nasrabadi, M.; Ahmadi, F. Application of carbon nanooxide- NiMoO_4 - MnWO_4 nanocomposite for modification of glassy carbon electrode: Electrochemical determination of ascorbic acid. *Microchem. J.* **2020**, *159*, 105470.
- (39) Ibarlucea, B.; Pérez Roig, A.; Belyaev, D.; Baraban, L.; Cuniberti, G. Electrochemical detection of ascorbic acid in artificial sweat using a flexible alginate/CuO-modified electrode. *Microchim. Acta* **2020**, *187*, 520–611.
- (40) Wang, Q.; Xiao, X.; Hu, X.; Huang, L.; Li, T.; Yang, M. Molecularly imprinted electrochemical sensor for ascorbic acid determination based on MXene modified electrode. *Mater. Lett.* **2021**, *285*, 129158.
- (41) Sharma, S.; Kumar, P.; Jabeen, S.; Samra, K. S. Hierarchical granular morphology of MoS_2 -RGO nanocomposite for electrochemical sensing of ascorbic-acid. *J. Mater. Sci.: Mater. Electron.* **2022**, *33*, 21048–21059.
- (42) Pei, S.; Zhang, J.; Gao, M.; Wu, D.; Yang, Y.; Liu, R. A facile hydrothermal approach towards photoluminescent carbon dots from amino acids. *J. Colloid Interface Sci.* **2015**, *439*, 129–133.